

MIT Open Access Articles

*A chirped-pulse Fourier-transform microwave/
pulsed uniform flow spectrometer. II. Performance
and applications for reaction dynamics*

The MIT Faculty has made this article openly available. **Please share** how this access benefits you. Your story matters.

Citation: Abeysekera, Chamara, Lindsay N. Zack, G. Barratt Park, Baptiste Joalland, James M. Oldham, Kirill Prozument, Nuwandi M. Ariyasingha, Ian R. Sims, Robert W. Field, and Arthur G. Suits. "A Chirped-Pulse Fourier-Transform Microwave/pulsed Uniform Flow Spectrometer. II. Performance and Applications for Reaction Dynamics." *The Journal of Chemical Physics* 141, no. 21 (December 7, 2014): 214203. © 2014 AIP Publishing.

As Published: <http://dx.doi.org/10.1063/1.4903253>

Publisher: American Institute of Physics (AIP)

Persistent URL: <http://hdl.handle.net/1721.1/96078>

Version: Final published version: final published article, as it appeared in a journal, conference proceedings, or other formally published context

Terms of Use: Article is made available in accordance with the publisher's policy and may be subject to US copyright law. Please refer to the publisher's site for terms of use.



A chirped-pulse Fourier-transform microwave/pulsed uniform flow spectrometer. II. Performance and applications for reaction dynamics

Chamara Abeysekera, Lindsay N. Zack, G. Barratt Park, Baptiste Joalland, James M. Oldham, Kirill Prozument, Nuwandi M. Ariyasingha, Ian R. Sims, Robert W. Field, and Arthur G. Suits

Citation: *The Journal of Chemical Physics* **141**, 214203 (2014); doi: 10.1063/1.4903253

View online: <http://dx.doi.org/10.1063/1.4903253>

View Table of Contents: <http://scitation.aip.org/content/aip/journal/jcp/141/21?ver=pdfcov>

Published by the [AIP Publishing](#)

Articles you may be interested in

[A chirped-pulse Fourier-transform microwave/pulsed uniform flow spectrometer. I. The low-temperature flow system](#)

J. Chem. Phys. **141**, 154202 (2014); 10.1063/1.4897979

[Reaction dynamics of O\(1D\) + HCOOD/DCOOH investigated with time-resolved Fourier-transform infrared emission spectroscopy](#)

J. Chem. Phys. **141**, 154313 (2014); 10.1063/1.4897418

[The complete iodine and nitrogen nuclear electric quadrupole coupling tensors for fluoroiodoacetonitrile determined by chirped pulse Fourier transform microwave spectroscopy](#)

J. Chem. Phys. **132**, 024310 (2010); 10.1063/1.3291619

[Infrared absorption of C₆H₅SO₂ detected with time-resolved Fourier-transform spectroscopy](#)

J. Chem. Phys. **126**, 134311 (2007); 10.1063/1.2713110

[Intermolecular potential-energy surface for the Ar-SH \(\$\pi\$ \) complex studied by Fourier-transform microwave spectroscopy](#)

J. Chem. Phys. **113**, 10121 (2000); 10.1063/1.1322364



A chirped-pulse Fourier-transform microwave/pulsed uniform flow spectrometer. II. Performance and applications for reaction dynamics

Chamara Abeysekera,¹ Lindsay N. Zack,¹ G. Barratt Park,² Baptiste Joalland,¹ James M. Oldham,¹ Kirill Prozument,¹ Nuwandi M. Ariyasingha,¹ Ian R. Sims,³ Robert W. Field,^{2,a)} and Arthur G. Suits^{1,a)}

¹Department of Chemistry, Wayne State University, 5101 Cass Avenue, Detroit, Michigan 48202, USA

²Department of Chemistry, Massachusetts Institute of Technology, Cambridge, Massachusetts 02139, USA

³Institut de Physique de Rennes, UMR CNRS-URI 6251, Université de Rennes 1, 263 Avenue du Général Leclerc, 35042, Rennes Cedex, France

(Received 15 October 2014; accepted 20 November 2014; published online 5 December 2014)

This second paper in a series of two reports on the performance of a new instrument for studying chemical reaction dynamics and kinetics at low temperatures. Our approach employs chirped-pulse Fourier-transform microwave (CP-FTMW) spectroscopy to probe photolysis and bimolecular reaction products that are thermalized in pulsed uniform flows. Here we detail the development and testing of a new K_a -band CP-FTMW spectrometer in combination with the pulsed flow system described in Paper I [J. M. Oldham, C. Abeysekera, B. Joalland, L. N. Zack, K. Prozument, I. R. Sims, G. B. Park, R. W. Field, and A. G. Suits, *J. Chem. Phys.* **141**, 154202 (2014)]. This combination delivers broadband spectra with MHz resolution and allows monitoring, on the μ s timescale, of the appearance of transient reaction products. Two benchmark reactive systems are used to illustrate and characterize the performance of this new apparatus: the photodissociation of SO_2 at 193 nm, for which the vibrational populations of the SO product are monitored, and the reaction between CN and C_2H_2 , for which the HCCCN product is detected in its vibrational ground state. The results show that the combination of these two well-matched techniques, which we refer to as chirped-pulse in uniform flow, also provides insight into the vibrational and rotational relaxation kinetics of the nascent reaction products. Future directions are discussed, with an emphasis on exploring the low temperature chemistry of complex polyatomic systems. © 2014 AIP Publishing LLC. [<http://dx.doi.org/10.1063/1.4903253>]

I. INTRODUCTION

Over the past several years there has been a burst of interest in microwave spectroscopy, due in part to the development of the chirped-pulse Fourier transform microwave (CP-FTMW) technique.¹ With this approach, a broadband microwave spectrum can be acquired more quickly than with traditional narrow band cavity FTMW methods, without greatly sacrificing dynamic range or signal-to-noise ratios. This increased *spectral velocity*—which we define as number of resolution elements acquired per unit time—also has the advantage of reducing sample consumption, and the shot-wise broadband scanning allows for reliable comparisons of line intensities for quantitative studies. These features have been demonstrated through the measurement of the pure rotational spectra of several complex organic molecules, with the goal of obtaining detailed structural information,² investigating tunneling and other intramolecular interactions concerning internal rotation,^{3–5} or generating data for astrophysical searches,⁶ for example. The flexibility of the CP approach has further been enhanced by the extension of its frequency range to the millimeter, submillimeter, and terahertz wavelength re-

gions, and in the implementation of novel data acquisition strategies.^{7–9}

The combination of detailed structural information that rotational spectroscopy affords, along with efficient signal acquisition spanning a broad spectral bandwidth, suggests that CP-FTMW offers compelling advantages for the study of reaction dynamics of polyatomic molecules. Indeed, Pate and co-workers have demonstrated that the broadband feature of CP-FTMW spectroscopy can be used to measure the rates of isomerization in laser-excited molecules,¹⁰ and more recently CP-FTMW/mmW has been used to probe the products generated from pyrolysis and photolysis reactions.^{11–14} Rotational spectroscopy techniques have been used for reaction dynamics and kinetics studies in the past,^{15–17} but have not been widely adopted. Traditional techniques, such as laser-induced fluorescence (LIF) or resonant multiphoton ionization (REMPI) methods, are still the preferred approaches for investigating reaction dynamics. CP microwave methods, with the broadband advantage, represent a tremendous advance, now making it possible to bring the structural specificity of rotational spectroscopy to bear on studies of reaction dynamics and kinetics. This advantage promises a new richness of detail for investigating the dynamics of polyatomic reactions. For large molecules, quantum-state specific REMPI and LIF schemes suitable for general application to

^{a)}Authors to whom correspondence should be addressed. Electronic addresses: rwfield@mit.edu and asuits@wayne.edu

reaction dynamics studies are largely unavailable. Nonresonant methods give ambiguous product identification because they produce broad, unstructured spectra. Product isomeric composition is undetermined, and branching ratios are rarely obtained accurately. Thus, one is unable to directly infer isomer and vibrational level specific information or branching. Synchrotron photoionization has emerged in recent years as a powerful isomer-selective detection strategy that has broad applicability, but it lacks detailed structural information and is only available at synchrotron facilities with somewhat limited access.^{18,19} In contrast, rotational spectroscopy can be used to differentiate between isomers, conformers, isotopologues, and vibrational states, even in mixtures. Moreover, the broadband detection scheme readily allows for comparison of relative line intensities of different species to provide accurate branching ratios if the products have a well-defined rotational temperature.¹¹ In a recent CP study, a signature of roaming dynamics was observed by quantifying branching into several reaction products aided by accurate kinetic modeling.¹⁴

As a form of rotational spectroscopy, CP-FTMW requires cold samples to produce sufficiently large population differences for sensitive spectroscopic detection. Molecular sources for CP-FTMW/mmW instruments are generally free jets based on pulsed solenoid valves, which provide rotationally cold samples when the gas is expanded into the vacuum chamber. However, these sources offer nonuniform environments where densities and temperatures can vary over several orders of magnitude throughout the flow. In addition, typically the total sample volume that may be interrogated is limited to a few cm^3 at product number densities of perhaps 10^{10} cm^{-3} . Moreover, the conditions in free jet expansions do not permit reactions or photochemistry to take place with the necessary rotational cooling under well-defined conditions. To overcome these challenges and provide uniform, well-defined flow conditions at low temperature and high density appropriate for reaction dynamics studies, we have chosen to couple the CP-FTMW technique to a pulsed uniform supersonic flow. In contrast to the free jet expansion, these flows can produce large volumes ($10\text{--}100 \text{ cm}^3$) of rotationally thermalized samples at temperatures of 20 K and product densities $>10^{14} \text{ cm}^{-3}$, ideal for CP-FTMW based detection. Our approach to generating pulsed uniform supersonic flows is based on an axisymmetric Laval nozzle and a novel high-throughput piezoelectric stack valve that has been described and characterized in Paper I.²⁰ The flow system has been developed and integrated into a new CP-FTMW spectrometer operating in the K_a -band (26–40 GHz).²⁰ We term this combination a Chirped-Pulse-Uniform Flow (CPUF) spectrometer. The system is also used with a mm-Wave spectrometer (60–90 GHz) based on one developed in the Field group^{8,11} but its performance is not described in this report.

Presented here is the second of two papers that describe this new approach. Following a description of the K_a -band spectrometer, examples illustrating the new instrument's capabilities are presented. In the first example, the 193 nm photofragmentation of SO_2 , yielding SO ($X^3\Sigma^-$), demonstrates how the CPUF system can be used to study photochemistry, detect product vibrational distributions, and track

rotational and vibrational relaxation accompanying photochemical processes. The second example shows that bimolecular reaction products produced in the uniform flow can be easily detected with this new method. A discussion of implications and prospects for this new technique is also provided.

II. EXPERIMENTAL

The new spectrometer consists of two main components as shown in Fig. 1: a K_a band (26–40 GHz) chirped-pulse Fourier-transform microwave setup²¹ and a Pulsed Uniform Flow (PUF) system described in detail in Paper I of Ref. 12, which is capable of producing a high density ($\sim 10^{17} \text{ cm}^{-3}$) and large volume of cold (20–30 K) molecules.

The CP-FTMW spectrometer consists of an 8 gigasamples/s arbitrary waveform generator (AWG; Tektronix AWG7082C) that produces microwave chirps having a linear frequency sweep up to 4 GHz in $\leq 1 \mu\text{s}$. The AWG pulse is upconverted in a broadband mixer (Marki M10418LC) with a phase-locked dielectric resonator oscillator (PDRO) operating at 8.125 GHz, and the mixer output is amplified by a broadband amplifier (ALC Microwave ALS030283). The frequency band is selected through a bandpass filter and propagated through a combination of active (Marki ADA8512K) and passive (Marki D0840L) frequency doublers to quadruple the linear sweep bandwidth in two stages. The final microwave pulse is amplified using a traveling wave tube (TWT; Applied System Engineering Inc. 187Ka) amplifier to obtain a peak power of 40 W. The pulse is directed through the PUF via a feedhorn mounted outside of the polycarbonate flow chamber and perpendicular to the flow, polarizing the molecules, which then undergo free induction decay (FID). The FID signal is collected with a second feedhorn and passed through a fast switch (Millitech PSH-28-SIAN0) that protects the low noise amplifier (LNA; Miteq JSDWK32) from the high-power microwave pulse. The LNA amplifies the weak FID signal, and the output is downconverted by a broadband mixer (Millitech MXP-28-RFSSL) with a PDRO operating at 16.75 GHz, multiplied with an active doubler (Marki ADA1020). The mixer output is sent to a digital oscilloscope (Tektronix DPO70804C) with a 25 gigasamples/s digitization rate and hardware bandwidths up to 8 GHz, where the FIDs from successive polarizing pulses are phase coherently averaged in the time domain, then fast-Fourier-transformed using a Kaiser-Bessel window function to obtain a frequency-domain spectrum. PDROs and the AWG are phase locked to a 10 MHz reference from a Rb-disciplined master clock (Stanford Research System FS725) to permit coherent averaging of the FID in the time domain. To reduce the phase drift of the oscillators, the PDROs and mixers are water cooled to 15 °C.

The vacuum chamber was constructed from a transparent polycarbonate tube (K-Mac Plastics) with inner diameter, length, and wall thickness of 24, 90, and 1 cm, respectively. This material minimizes reflections from the microwave radiation, decreasing the possibility of creating standing waves. Two aluminum flanges seal the transparent tube. The Laval nozzle is mounted on one flange, while the other is attached to the turbomolecular pump assembly. The chamber is mounted

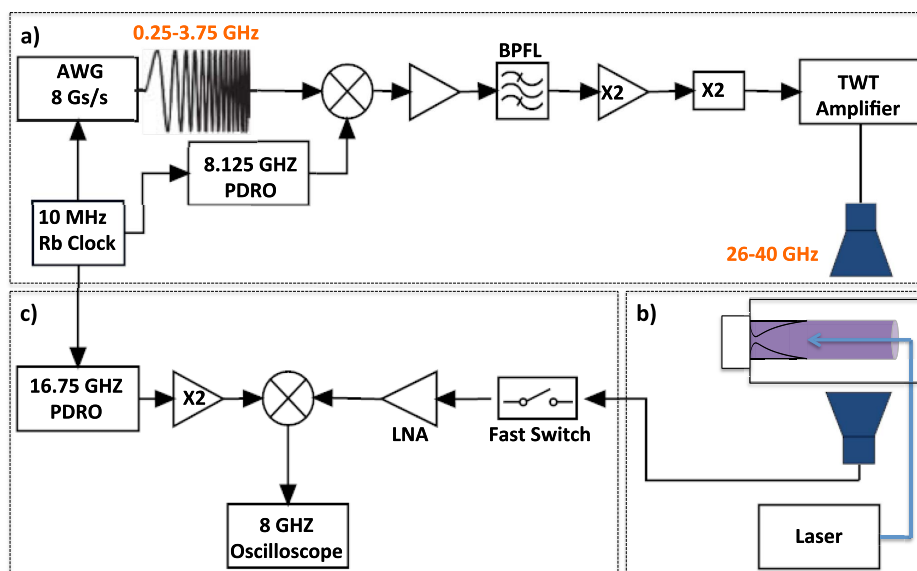


FIG. 1. The CPUF setup is illustrated in three parts: (a) Chirped pulses (0.25–3.75 GHz) are produced in an arbitrary waveform generator (AWG) and then mixed with a LO frequency (8.125 GHz) locked to a 10 MHz Rb standard. The resulting frequencies are then multiplied ($4\times$) via a series of active and passive doublers before further amplification by a 40 W traveling wavetube amplifier (TWT). The microwave radiation is then broadcast through the molecular sample via a feedhorn oriented perpendicular to the molecular axis. Bandpass filters and isolators are inserted into the setup as necessary. (b) A piezoelectric stack valve and Laval nozzle are mounted on one end of a polycarbonate vacuum chamber.²⁰ A quartz window is located on the other end of the chamber to allow radiation from an excimer laser to propagate down the axis of the Laval nozzle, such that the core of the flow is irradiated. (c) Molecular emission in the form of free induction decay (FID) is collected by a second feedhorn. This signal is downconverted before detection and phase coherently averaged in an oscilloscope, where it is fast Fourier-transformed to produce a frequency-domain spectrum.

onto a translation stage, which enables linear movement of the chamber such that different regions of the flow can be probed without disturbing the microwave and antenna setup.

A quartz window is mounted into the chamber attached to the turbomolecular pump. Through this window, the output from an excimer laser, operating at either 193 or 248 nm (GAM Laser, EX200/60), is directed through the vacuum chamber and down the axis of the flow. The laser beam is loosely focused with a biconvex lens ($f = 200$ cm) to a width of approximately 5 mm at the throat of the Laval nozzle.

The timing for the experiment is controlled by the AWG, which has two main output (marker) channels. The AWG output is routed through two pulse-delay generators (Berkeley Nucleonics Corp. Model #555 and 575), one of which is used to control the delays between the gas pulse and laser relative to the chirp sequence. The other delay generator sets the timings of the TWT amplification and the fast PIN switch. All timing delays are optimized for the system being studied to ensure that reactions occurring in the flow are studied. Typically we record many chirp-FID sequences in each gas pulse.

III. RESULTS

The newly commissioned CPUF spectrometer was initially tested and benchmarked with OCS to evaluate its overall performance. The CPUF results were comparable to those previously published for a K_a -band CP-FTMW spectrometer.²¹ Because the CPUF spectrometer has been developed and designed for the purpose of studying chemical reaction dynamics, some well-known systems were chosen to

demonstrate this new spectrometer's capabilities for that application. These examples illustrate the versatility of this instrument and its utility as a complementary method relative to traditional approaches. We first present signal level estimates, and then provide examples to illustrate the performance.

A. Estimating signal levels

The signal detected by the CP-FTMW spectrometer is the electric field of the FID of the polarized molecules. From the expression derived by McGurk *et al.*²² for the polarization resulting from adiabatic fast passage, the measured signal, E_{FID} , is given by

$$E_{\text{FID}} \propto \omega \mu^2 E_{\text{pulse}} \Delta N (\pi/\alpha)^{1/2},$$

where ω is the frequency, μ the transition dipole moment, E_{pulse} the electric field strength of the pulse, ΔN the population difference, and α the linear sweep rate. The spectral resolution of the collected signal depends only on the duration of the collected FID, not on the excitation pulse duration.

A unique consideration of performing CP microwave spectroscopy in flows is the possible attenuation of line intensities in the spectra due to the impact of collisions; this effect is not a concern under free-jet expansions, as the CP probe is employed in the “collision-free” region in that case. Under the conditions prevailing in our helium flow, $P = 0.18$ Torr and $T = 22$ K, we estimate a mean free path of $\lambda = 30$ μm and a collision frequency of roughly 11 MHz, implying a mean time between collisions of ~ 90 ns, shorter than the typical chirp durations in CPUF. Thus, transitions excited early in the pulse are likely to undergo collisions, possibly attenuating the line intensities, while transitions excited later do

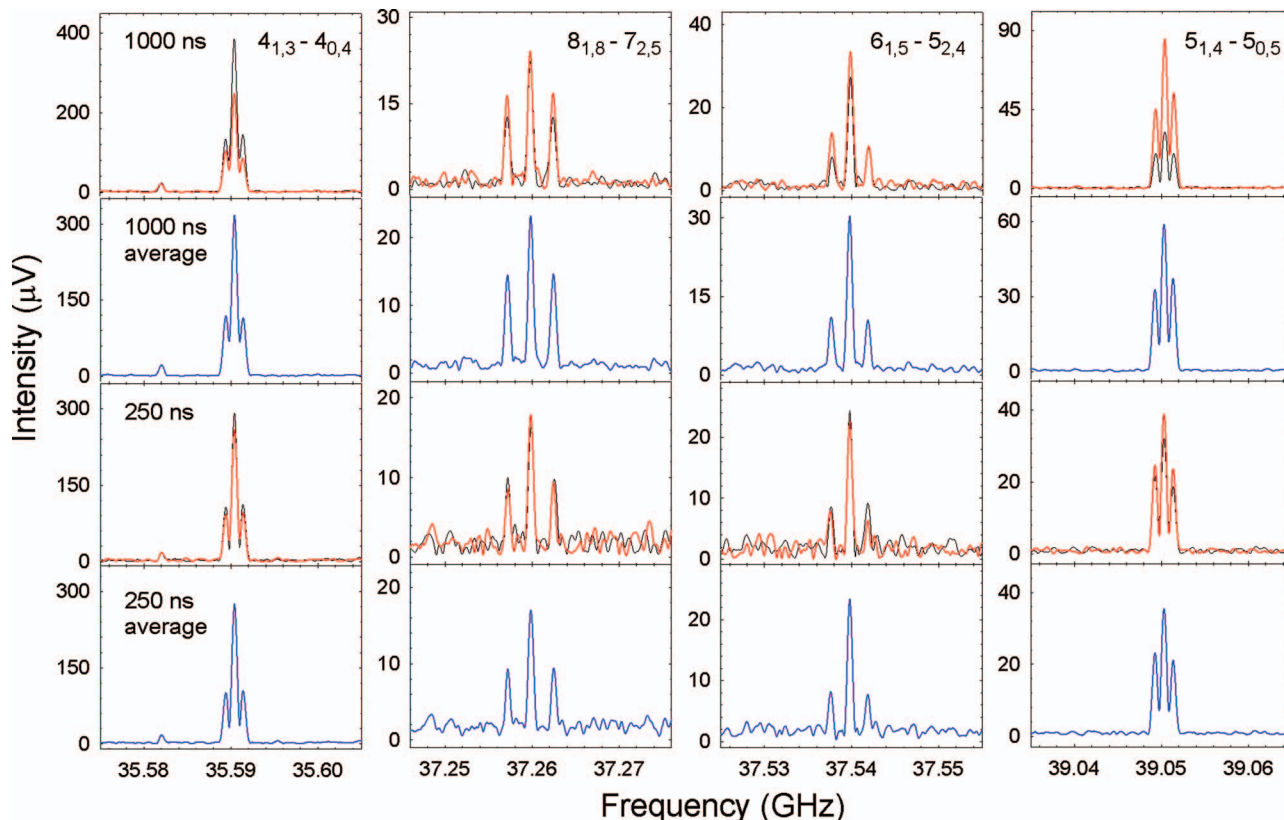


FIG. 2. Several rotational transitions of dimethyl ether ($J'_{Ka',Kc'}-J''_{Ka'',Kc''}$) over the 34–40 GHz frequency range are shown to illustrate the effects of collisional dephasing on signal intensities. The top row of spectra was taken with chirp duration of 1000 ns, and a clear asymmetry exists in the line intensities between up- (red trace) or down-swept (black) frequencies. This asymmetry is less severe in spectra obtained with a 250 ns chirp duration (middle row) or shorter. Averaging up- and down-chirped spectra can compensate for the dephasing effects, as shown in rows two and four (blue traces) for the 1000 and 250 ns spectra, respectively. Each spectrum is an average of roughly 100 000 acquisitions, which took ~ 5 min of integration time at a pulsed valve repetition rate of 3.3 Hz, with 200 acquisitions collected per gas pulse.

not display this loss of signal. Shown in Fig. 2 are several dimethyl ether transitions in the frequency region 34–40 GHz with 1000 and 250 ns chirps swept either down (black trace) or up (red) in frequency. A clear asymmetry in line intensities is apparent in the 1000 ns spectra, but not in the 250 ns spectra. This effect implies that relative line intensities across the swept bandwidth may not necessarily be reliable for the longer chirp. Some compensation for this effect can be obtained, however, by averaging upchirp and downchirp spectra in the frequency domain (Fig. 2, second and bottom rows, blue traces). Of course, this asymmetry can be overcome by using a chirp duration shorter than the collision time scale, but at the cost of a significant sacrifice in signal strength.

The spectrometer capabilities are illustrated in Fig. 3 with the closed-shell linear molecule OCS, which has a dipole moment $\mu = 0.715$ D and a rotational constant $B = 6081.492$ MHz. The spectrum was collected over a 6 GHz frequency range (34–40 GHz), with a chirp duration of 1 μ s. A sample of 1% OCS in helium was used to evaluate the sensitivity of the instrument through the detection of the most abundant isotopologue ($^{16}\text{O}^{12}\text{C}^{32}\text{S}$, 93.74%), as well as OC^{34}S (4.158%), O^{13}CS (1.053%), and OC^{33}S (0.740%), with its hyperfine splittings.²¹ The signal stability and the signal-to-noise ratio (S/N) were checked by comparing single- and 10 000-shot $^{16}\text{O}^{12}\text{C}^{32}\text{S}$ spectra of the $J = 3-2$ rotational transition at 36.488 GHz. This peak showed an increase

in S/N by a factor of 85 with a peak intensity of 2.308 mV and line width of 0.6 MHz after 10 000 acquisitions. The population difference (ΔN) at 22 K can then be calculated using the partition function of O^{12}CS , the sample density (4×10^{14} cm^{-3}), a probe core volume of 5 cm^3 (based on an 8 mm diameter, 10 cm long flow) yielding a rotational level population difference of $\Delta N = 7.6 \times 10^{12}$ molecules in the irradiated volume.

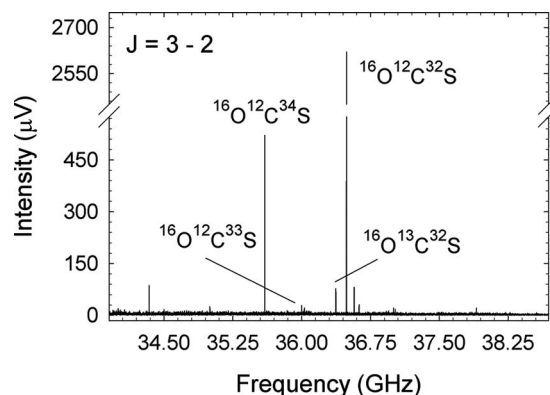


FIG. 3. A representative broadband spectrum of the isotopologues of OCS ($\bar{X}^1\Sigma^+$) in the $J = 3-2$ transition near 36 GHz is shown. The break in the y-axis allows the full intensity of the main isotopologue, $^{16}\text{O}^{12}\text{C}^{32}\text{S}$, to be shown. The ^{33}S nuclear spin ($I = 3/2$) splits the weaker $^{16}\text{O}^{12}\text{C}^{33}\text{S}$ line into $2I + 1$ components. The spectrum is an average of ~ 10 000 shots.

The signal intensity of OCS can be used as a benchmark and basis for comparison to estimate the expected signal levels for photodissociation or bimolecular reactions in the flow. We first estimate these for the reactions we examine below. The flow density of the Laval system with He as the carrier gas is $4 \times 10^{16} \text{ cm}^{-3}$. If the 193 nm photodissociation of SO_2 to yield $\text{SO} (X^3\Sigma^-)$ is considered, we can estimate ΔN for the product SO as follows. At 193 nm, 10 mJ/pulse corresponds to $\sim 10^{16}$ photons per pulse. Using the SO_2 absorption cross section (10^{-17} cm^2) and an SO_2 density of $4 \times 10^{14} \text{ cm}^{-3}$, assuming unit quantum yield for dissociation, we produce 4×10^{13} product molecules per cm of path length. For the 10 cm long interaction volume, analogous to OCS, this gives a total of 4×10^{14} molecules in a volume of 5 cm^3 , or a density of $8 \times 10^{13} \text{ cm}^{-3}$. Taking into account the Boltzmann factor, we obtain a total population difference $\Delta N = 3 \times 10^{11}$, roughly a factor of twenty smaller than that of OCS. The dipole moment of SO is $\mu = 1.55 \text{ D}$, so for the $N_J = 1_0 - 0_1$ transition in the $v'' = 0$ vibrational level at 30.001 GHz, a signal level a factor of five lower than that of O^{12}CS can be anticipated. In this case the larger dipole moment and partition function of ~ 20 compensate for the fraction ($\sim 10\%$) of the molecules undergoing photodissociation. However, one must also account for the relative intensities of the fine structure components when studying open-shell molecules. In the case of SO, the $N = 1 - 0$ rotational transition splits into three spin components corresponding to the $N_J = 1_0 - 0_1$, $1_2 - 0_1$, and $1_1 - 0_1$ transitions. From the calculated line strengths of each transition, only about 8% of the SO population is expected to be observed in the $N_J = 1_0 - 0_1$, as opposed to 61% and 31% in $N_J = 1_2 - 0_1$ and $1_1 - 0_1$, respectively. Thus, contributions of all spin components must be considered when calculating the SO signal levels.

For a bimolecular reaction, the product yield can also be estimated as above, with the flow density of $4 \times 10^{16} \text{ cm}^{-3}$ at 22 K. For the reaction of the CN radical with acetylene (C_2H_2) to produce cyanoacetylene (HCCCN), 1.5% C_2H_2 and 1% BrCN as a CN precursor were used. The CN concentration can again be estimated using the initial BrCN density of $4 \times 10^{14} \text{ cm}^{-3}$ and an absorption cross-section of 10^{-18} cm^2 at 193 nm. Here we use 40 mJ/pulse with 10 cm flow length to give an estimated a total of 1.6×10^{13} CN radicals per cm of path length. Assuming unit reaction efficiency between CN and acetylene, and the 10 cm path length, we estimate that approximately 1.6×10^{14} HCCCN molecules will be produced, corresponding to a density of $3.2 \times 10^{13} \text{ cm}^{-3}$. Given the second order rate constant $k = 4 \times 10^{-10} \text{ cm}^3 \text{ molecules}^{-1} \text{ s}^{-1}$ at 25 K,²³ we anticipate reaction in the flow on a timescale of $\sim 5 \mu\text{s}$. The HCCCN product will also react with CN with a rate constant of $1 \times 10^{-10} \text{ cm}^3 \text{ molecules}^{-1} \text{ s}^{-1}$ at 22 K to give dicyanoacetylene,²³ but simple simulations show that this will not significantly affect the final HCCCN concentration. Considering a dipole moment of $\mu = 3.73 \text{ D}$ for HCCCN and the rotational level population difference $\Delta N = 1.9 \times 10^{12}$ molecules in the irradiated volume, an estimate for the signal level of the $J = 4-3$ rotational transition at 36.392 GHz can be obtained. Thus, the expected signal intensity of HCCCN should be an order of magnitude larger than that of OCS, with the assumed reaction

efficiency of 100% is a single product vibrational level were populated.

B. Photochemistry: $\text{SO}_2 + h\nu (193 \text{ nm}) \rightarrow \text{O} (^3\text{P}_J) + \text{SO} (X^3\Sigma^-, v)$

The 193 nm photodissociation of SO_2 has been previously studied by several different methods, including velocity map imaging, Fourier-transform infrared spectroscopy, microwave spectroscopy, and laser induced fluorescence spectroscopy.^{17,24-29} From those experiments, it was concluded that this reaction occurs via excitation from the ground \tilde{X}^1A_1 state to the \tilde{C}^1B_2 state followed by dissociation. However, the \tilde{C} state correlates diabatically to singlet fragments, $\text{SO} (a^1\Delta)$ and $\text{O} (^1\text{D})$, rather than the observed triplets, $\text{SO} (X^3\Sigma^-)$ and $\text{O} (^3\text{P})$, so other pathways must participate. The dominant process is thought to be internal conversion arising when mixing occurs between the quasibound continuum of the \tilde{X} ground state with vibronic levels in the \tilde{C} state, but dissociation via a triplet surface could also result from the crossing of the \tilde{C} state by repulsive $2^3A'$ or $3^1A'$ states.^{24,25,27,30} These conclusions were drawn, in part, from the observation of inverted vibrational distributions in the SO fragment, where $>50\%$ of the population is in the $v'' = 2$ vibrational level rather than the ground $v'' = 0$ state (Table I).^{24,26,27,31}

The CPUF spectrometer was used to probe the nascent vibrational distribution of SO following photodissociation of SO_2 . The SO_2 (Sigma Aldrich, 99.9%) was seeded at 0.5% in the helium flow and dissociated using an ArF excimer laser. To monitor the appearance of the product, the “fast-frame” capability of the oscilloscope was used,^{7,11} such that successive spectra were obtained at $5 \mu\text{s}$ intervals following an initial $10 \mu\text{s}$ delay between the laser trigger and the first chirped pulse excitation. Ten frames (i.e., spectra) obtained in this fashion, each an average of roughly 6500 acquisitions, are shown in Fig. 4. The spectra are stacked such that the top and bottom frames show the spectra collected at 20 and $65 \mu\text{s}$ after the laser is fired, respectively. Each frame shows the $N_J = 1_0 - 0_1$ pure rotational transition of SO in the $v'' = 2, 1$, and 0 vibrational levels near 30 GHz; other fine structure components of the $N = 1 - 0$ transition lie outside of the spectrometer’s immediate frequency range. A small Zeeman

TABLE I. Nascent vibrational distributions of $\text{SO} (X^3\Sigma^-)$ from the 193 nm photodissociation of SO_2 .

v''	Population (%)			
	REMPI + VMI ^a	LIF ^b	IR ^c	CPUF ^d
0	9	2	...	20
1	23	20	20	21
2	56	83	70	58
3	6	0
4	6
5	<10	...

^aReference 24.

^bReference 26; $\text{SO} A^3\Pi \rightarrow X^3\Sigma^-$ transition probed from 255 – 295 nm.

^cReference 31; tunable infrared diode-laser spectroscopy.

^dThis work; vibrational distribution 25 μs after the laser was fired.

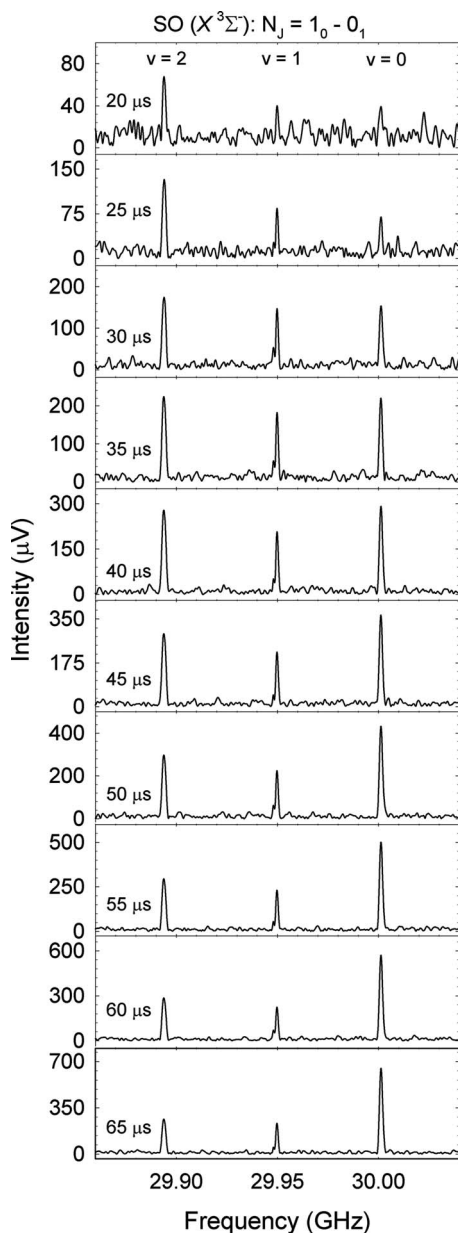


FIG. 4. SO_2 was irradiated with 193 nm radiation to produce SO ($X^3\Sigma^-$) in its $v'' = 0, 1,$ and 2 vibrational states. Shown here are spectra of the SO $N_j = 1_0 - 0_1$ rotational transition to illustrate the vibrational cooling of this photofragment over a $65 \mu\text{s}$ time frame. Times shown on the spectra are the time of the chirp after the firing of the laser. Initially, most of the SO population is in the $v'' = 2$ level, consistent with the nascent distribution determined from imaging studies, followed by fast relaxation to the $v'' = 0$ level. Each spectrum was collected over the frequency range 29.3–30.1 GHz using an upchirp with a $1 \mu\text{s}$ duration and is an average of 6500 acquisitions.

splitting caused by the interaction with the Earth's magnetic field is visible on some of the lines as well.

The $v'' = 2$ level clearly dominates when the SO product first appears (see also Table I), consistent with previous studies, but rapid vibrational quenching to the $v'' = 0$ state follows. Fig. 5, which shows the populations of each vibrational state at different time points, illustrates this effect as well. It should be mentioned, however, that measurement of higher rotational states could also provide valuable insight, as it has been noted that there is a shift in population toward

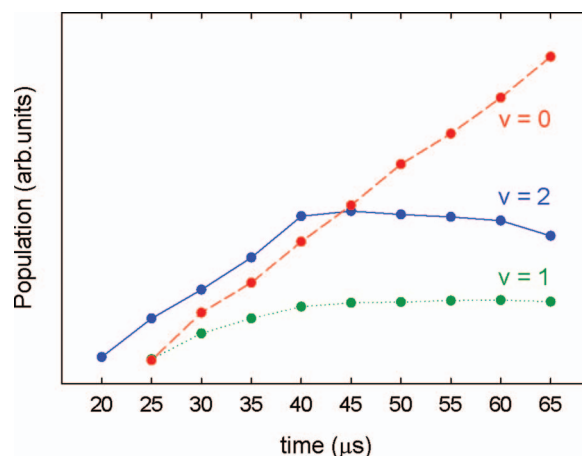


FIG. 5. The populations of the $v'' = 2, 1,$ and 0 vibrational levels of SO ($X^3\Sigma^-$) are shown over time. Initially, only SO in the $v'' = 2$ state is present ($t = 20 \mu\text{s}$); S/N was not high enough to get reliable $v'' = 1$ and 0 populations at this time point. SO in the $v'' = 1$ state remains fairly constant over $65 \mu\text{s}$, while $v'' = 0$ shows a large increase over time, due to fast vibrational cooling and possible v-v effects.

higher rotational levels in lower vibrational levels.^{28,31,32} The very rapid vibrational relaxation observed here is likely owing to the near resonance of the SO fundamental (1149 cm^{-1}) with the SO_2 symmetric stretch (1151 cm^{-1}), possibly giving rise to very efficient v-v energy transfer.¹⁸ The fact that $v'' = 2$ continues to dominate over $v'' = 1$ even as $v'' = 0$ becomes dominant is a puzzling feature that may be the result of additional underlying resonant relaxation pathways. Although beyond the scope of the present study, this shows the potential of the method to explore such phenomena.

A more in-depth study could investigate the competition between rotational and vibrational cooling of SO fragments or probe vibration-vibration interactions between parent and daughter species, however that is beyond the scope of this report. Nonetheless, this work shows that the CPWF spectrometer can be used to monitor nascent vibrational distributions and track vibrational and rotational relaxation kinetics.

C. Bimolecular reactions: $\text{CN} + \text{C}_2\text{H}_2 \rightarrow \text{HCCCN} + \text{H}$

A distinct advantage of using a PUF system as the molecular source for this spectrometer is that it provides a high-density molecular flow at constant pressure and uniform low temperature. This feature offers the capability to initiate bimolecular reactions in the flow with a large enough number of product molecules in the probed volume, and with collisions to thermalize the molecules to uniform low rotational temperature quickly, so that CP microwave spectroscopy may be effectively employed as a probe. At the same time, it becomes possible to monitor the kinetics of these reactions, as we saw above for vibrational relaxation kinetics in SO . This combined system of broadband rotational spectroscopy in a PUF offers complementary capabilities when compared to the crossed-molecular beam approach to reaction dynamics studies. It allows for investigation of all the product channels for polyatomic molecules that possess an electric dipole moment and have rotational transitions within a desired

frequency window in a single spectrum, so accurate product vibrational branching ratios can be measured. Further, microwave spectroscopy can reveal detailed isomeric identity and structural information. It does not offer differential cross sections or translational energy distributions, but for larger and more complex systems, these differential measurements generally lack detail and offer somewhat limited insight. It is important to note, though, that these are necessarily not single-collision conditions, so competing reactions and alternative chemistry must always be borne in mind in interpreting the results.

There has been much speculation about the formation pathways of cyanopolyynes due to their importance in astrochemistry. Detection of this class of molecules in a wide variety of astrophysical environments^{33–36} has led to the proposal that ion-molecule and dissociative recombination mechanisms or neutral-neutral reactions might be responsible for their presence in interstellar gas.³⁷ Low temperature CRESU [Reaction Kinetics in Uniform Supersonic Flow (in French)] kinetics measurements support the latter by showing that a neutral-neutral reaction between cyano radical, CN, and an acetylenic chain, such as C_2H_2 in the simplest case, could be very facile.²³ Such a reaction would proceed via an attack by the CN radical on a π orbital of C_2H_2 to create a C_2H_2CN complex, followed by a bond rupture to produce HCCCN and H, with these products lying at 90 kJ mol^{-1} lower enthalpy than the reactants.

To demonstrate the capabilities of the instrument to study bimolecular reactions, the $CN + C_2H_2$ reaction was investigated in the CPUF instrument. A mixture containing 1.5% C_2H_2 and 1% BrCN seeded in He (with 5% H_2 added to promote rotational cooling) was introduced into the chamber. Irradiation by a 40 mJ/pulse at 193 nm photodissociated the BrCN to produce CN radicals. BrCN photodissociation at 193 nm has been shown to produce rotationally hot but vibrationally quite cold CN.³⁸ We believe the observed induction time discussed below may partially reflect rotational relaxation prior to reaction. Only the molecular product, HCCCN, was expected in the spectrum; neither of the reactants was observable because of lack of permanent dipole moment (C_2H_2) or having rotational transitions in a frequency window not accessible by our spectrometer (CN). HCCCN has several transitions in the spectrometer's frequency range, corresponding to $J = 3 - 2$ and $4 - 3$ rotational transitions in the ground and several low-lying excited vibrational states. However, only the $v = 0$ states near 27.3 and 34.4 GHz were targeted and observed using short chirp bandwidths to optimize the signal. Spectra of the $J = 4 - 3$ pure rotational transition of HCCCN in its vibrational ground state, produced from the reaction of $C_2H_2 + CN$, are shown in Fig. 6. Here spectra collected at successive $10 \mu\text{s}$ intervals up to $110 \mu\text{s}$ following the laser trigger show that HCCCN appears roughly $40 \mu\text{s}$ after the laser fires. The inset in Fig. 6 tracks the time dependence of HCCCN, and shows an onset at $40 \mu\text{s}$ and modest increase to about $70 \mu\text{s}$, after which there is a sharper increase before decaying after $90 \mu\text{s}$. The apparent delay in HCCCN's initial appearance is likely due to the need for rotational cooling, similar to that seen in the SO_2 photochemistry study, while the more abrupt rise at $70 \mu\text{s}$ likely represents re-

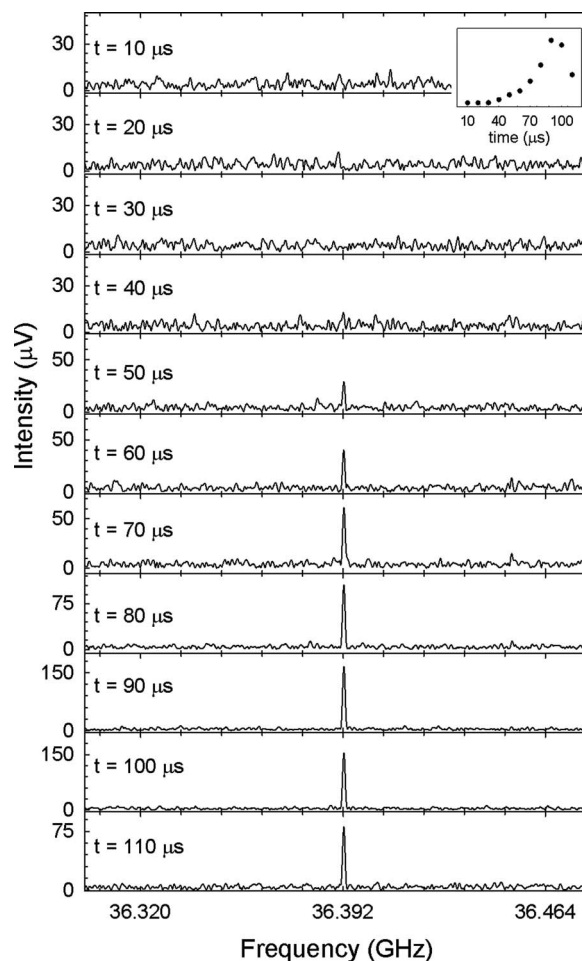


FIG. 6. Spectra illustrating the time evolution of the $J = 4 - 3$ rotational transition of HCCCN ($\tilde{X}^1\Sigma^+$), generated via the bimolecular reaction of the CN ($X^2\Sigma^+$) radical and C_2H_2 ($\tilde{X}^1\Sigma^+$), are displayed. The CN radical was produced by irradiation of BrCN with a 193 nm laser. HCCCN appears approximately $40\text{--}50 \mu\text{s}$ after the laser is fired. The inset shows the integrated intensity of the HCCCN line at each time point, with the peak intensity occurring at $\sim 90 \mu\text{s}$. Each spectrum is an average of 22 000 acquisitions obtained over the frequency range 35.25–36.45 GHz using a $1 \mu\text{s}$ duration upchirp.

actions that occur at the much higher densities present in the throat of the nozzle. This is confirmed by an estimate of the flow velocity of 1500 m s^{-1} and the distance of the throat to the center of the horns of 12 cm, implying arrival of products from the high density region $80 \mu\text{s}$ after photolysis.

Rate constants have been measured for other reactions involving CN and hydrocarbons such as C_2H_6 , C_2H_4 , and C_2H_2 using the CRESU apparatus at 25 K under uniform flow conditions.²³ Using these rate constants for CPUF conditions, the product formation time scales are expected to be on the order of tens of microseconds, making them suitable targets for CPUF. Moreover, reactions involving related carbon chain systems may yield multiple products with significant dipole moments, enabling measurement of product branching ratios.

IV. CONCLUSIONS AND OUTLOOK

A new K_a -band chirped pulse Fourier-transform microwave spectrometer has been constructed for the purpose of investigating molecular reaction dynamics and kinetics. This

spectrometer uses a high-throughput piezoelectric stack valve and a Laval nozzle to generate well-collimated high-density cold flows, such that photochemistry and bimolecular reactions can be initiated and the products thermalized with large volumes at high density. The spectral velocity advantage of the chirped pulse microwave technique allows for the efficient simultaneous measurement of several spectral lines with reliable intensity ratios, making it possible to establish accurate branching ratios if many species are present. To demonstrate the spectrometer's capabilities, two well-known systems were chosen for study—the 193 nm photodissociation of SO₂ and the reaction between C₂H₂ and CN. These examples show the power of this instrument for studies of photochemistry and bimolecular reactions. This new technique should be complementary to traditional techniques for studying reaction dynamics, especially for systems involving small polyatomic molecules.

The main challenge with this new method is the generation of sufficient reaction products to obtain adequate signal intensities. Increasing the reactant concentration could aid in this goal, however this will also lead to more clustering or quenching in the flow, effectively attenuating the signal. Two other avenues to increased signal are greater photolysis laser power, which is readily achieved, and larger nozzles for larger flow volumes, which can also be implemented fairly easily. We have demonstrated larger flows of longer duration with an argon nozzle, but it appears that clustering in an argon flow inhibits achievement of adequate concentrations. We plan to develop a helium/neon nozzle that may represent an optimum compromise for density, volume, and collision frequency.

Despite these challenges, the promise of CPUF is considerable. Photochemistry with complex and competing product branching represents an important initial direction. Further bimolecular reactions between the cyano radical and various hydrocarbons have been studied from both experimental and theoretical perspectives, but questions still remain regarding product branching ratios.^{39–41} These reactions are also attractive targets for CPUF because, in many cases, the microwave spectra of the products are already known and the relevant species have large electric dipole moments. Other systems targeted for future CPUF investigations are Criegee intermediates and QOOH products or reactions of the methylidyne radical (CH) with small hydrocarbons. Just as with the Criegee compounds, the ability to cool and trap molecules as transient intermediates holds promise for new insights into the role of such species in reaction dynamics. CPUF is an ideal instrument with which to pursue such studies.

ACKNOWLEDGMENTS

The National Science Foundation (NSF), Award MRI-ID 1126380, supported this work. I.R.S. thanks the CNRS and the Université de Rennes 1 for funding to support this collaboration.

¹G. G. Brown, B. C. Dian, K. O. Douglass, S. M. Geyer, S. T. Shipman, and B. H. Pate, *Rev. Sci. Instrum.* **79**, 053103 (2008).

- ²J. L. Neill, S. T. Shipman, L. Alvarez-Valtierra, A. Lesarri, Z. Kisiel, and B. H. Pate, *J. Mol. Spectrosc.* **269**, 21 (2011).
- ³H. V. L. Nguyen, I. Kleiner, S. T. Shipman, Y. Mae, K. Hirose, S. Hatanaka, and K. Kobayashi, *J. Mol. Spectrosc.* **299**, 17 (2014).
- ⁴B. Reinhold, I. A. Finneran, and S. T. Shipman, *J. Mol. Spectrosc.* **270**, 89 (2011).
- ⁵I. A. Finneran, S. T. Shipman, and S. L. Widicus Weaver, *J. Mol. Spectrosc.* **280**, 27 (2012).
- ⁶J. A. Kroll, S. T. Shipman, and S. L. Widicus Weaver, *J. Mol. Spectrosc.* **295**, 52 (2014).
- ⁷A. L. Steber, B. J. Harris, J. L. Neill, and B. H. Pate, *J. Mol. Spectrosc.* **280**, 3 (2012).
- ⁸G. B. Park, A. H. Steeves, K. Kuyanov-Prozument, J. L. Neill, and R. W. Field, *J. Chem. Phys.* **135**, 024202 (2011).
- ⁹E. Gerecht, K. O. Douglass, and D. F. Plusquellic, *Opt. Express* **19**, 8973 (2011).
- ¹⁰B. C. Dian, G. G. Brown, K. O. Douglass, and B. H. Pate, *Science* **320**, 924 (2008).
- ¹¹K. Prozument, G. B. Park, R. G. Shaver, A. K. Vasiliou, J. M. Oldham, D. E. David, J. S. Muentner, J. F. Stanton, A. G. Suits, G. B. Ellison, and R. W. Field, *Phys. Chem. Chem. Phys.* **16**, 15739 (2014).
- ¹²N. M. Kidwell, V. Vaquero-Vara, T. K. Ormond, G. T. Buckingham, D. Zhang, D. N. Mehta-Hurt, L. McCaslin, M. R. Nimlos, J. W. Daily, B. C. Dian, J. F. Stanton, G. B. Ellison, and T. S. Zwier, *J. Phys. Chem. Lett.* **5**, 2201 (2014).
- ¹³K. Prozument, R. G. Shaver, M. A. Ciuba, J. S. Muentner, G. B. Park, J. F. Stanton, H. Guo, B. M. Wong, D. S. Perry, and R. W. Field, *Faraday Discuss.* **163**, 33 (2013).
- ¹⁴K. Prozument, Y. V. Suleimanov, B. Buesser, J. M. Oldham, W. H. Green, A. G. Suits, and R. W. Field, *J. Phys. Chem. Lett.* **5**, 3641 (2014).
- ¹⁵N. Yoshida and S. Saito, *Bull. Chem. Soc. Jpn.* **51**, 1635 (1978).
- ¹⁶Y. Endo, S. Tsuchiya, C. Yamada, E. Hirota, and S. Koda, *J. Chem. Phys.* **85**, 4446 (1986).
- ¹⁷S. Koda, Y. Endo, S. Tsuchiya, and E. Hirota, *J. Phys. Chem.* **95**, 1241 (1991).
- ¹⁸A. G. Suits, *Chemical Applications of Synchrotron Radiation. Part I: Dynamics and VUV Spectroscopy. Part II: X-Ray Applications* (World Scientific Publishing Co. Pte. Ltd., Singapore, 2002), pp. 3–54.
- ¹⁹S. R. Leone, M. Ahmed, and K. R. Wilson, *Phys. Chem. Chem. Phys.* **12**, 6564 (2010).
- ²⁰J. M. Oldham, C. Abeysekera, B. Joalland, L. N. Zack, K. Prozument, I. R. Sims, G. B. Park, R. W. Field, and A. G. Suits, *J. Chem. Phys.* **141**, 154202 (2014).
- ²¹D. P. Zaleski, J. L. Neill, M. T. Muckle, N. A. Seifert, P. Brandon Carroll, S. L. Widicus Weaver, and B. H. Pate, *J. Mol. Spectrosc.* **280**, 68 (2012).
- ²²J. C. McGurk, T. G. Schmalz, and W. H. Flygare, *J. Chem. Phys.* **60**, 4181 (1974).
- ²³I. R. Sims, J.-L. Queffelec, D. Travers, B. R. Rowe, L. B. Herbert, J. Karthäuser, and I. W. Smith, *Chem. Phys. Lett.* **211**, 461 (1993).
- ²⁴M. Brouard, R. Cireasa, A. P. Clark, T. J. Preston, C. Vallance, G. C. Groenenboom, and O. S. Vasutiniskii, *J. Phys. Chem. A* **108**, 7965 (2004).
- ²⁵B. R. Cosofret, S. M. Dylewski, and P. L. Houston, *J. Phys. Chem. A* **104**, 10240 (2000).
- ²⁶X. Chen, F. Asmar, H. Wang, and B. R. Weiner, *J. Phys. Chem.* **95**, 6415 (1991).
- ²⁷H. Katagiri, T. Sako, A. Hishikawa, T. Yazaki, K. Onda, K. Yamanouchi, and K. Yoshino, *J. Mol. Struct.* **413–414**, 589 (1997).
- ²⁸S. Becker, C. Braatz, J. Lindner, and E. Tiemann, *Chem. Phys.* **196**, 275 (1995).
- ²⁹N. Hansen, U. Andresen, H. Dreizler, J.-U. Grabow, H. Mäder, and F. Temps, *Chem. Phys. Lett.* **289**, 311 (1998).
- ³⁰J. Ma, M. J. Wilhelm, J. M. Smith, and H.-L. Dai, *J. Phys. Chem. A* **116**, 166 (2012).
- ³¹H. Kanamori, J. E. Butler, K. Kawaguchi, C. Yamada, and E. Hirota, *J. Chem. Phys.* **83**, 611 (1985).
- ³²C. Braatz and E. Tiemann, *Chem. Phys.* **229**, 93 (1998).
- ³³J. R. Pardo, J. Cernicharo, J. R. Goicoechea, M. Guélin, and A. Asensio Ramos, *Astrophys. J.* **661**, 250 (2007).
- ³⁴G. Winnewisser and C. M. Walmsley, *Astron. Astrophys.* **70**, L37 (1978).

- ³⁵M. B. Bell, P. A. Feldman, M. J. Travers, M. C. McCarthy, C. A. Gottlieb, and P. Thaddeus, *Astrophys. J.* **483**, L61 (1997).
- ³⁶N. W. Broten, T. Oka, L. W. Avery, J. M. MacLeod, and H. W. Kroto, *Astrophys. J.* **223**, L105 (1978).
- ³⁷Y. Osamura, K. Fukuzawa, R. Terzieva, and E. Herbst, *Astrophys. J.* **519**, 697 (1999).
- ³⁸C. Huang, W. Li, R. Silva, and A. G. Suits, *Chem. Phys. Lett.* **426**, 242 (2006).
- ³⁹C. J. Bennett, S. B. Morales, S. D. Le Picard, A. Canosa, I. R. Sims, Y. H. Shih, A. H. H. Chang, X. Gu, F. Zhang, and R. I. Kaiser, *Phys. Chem. Chem. Phys.* **12**, 8737 (2010).
- ⁴⁰L. C. L. Huang, Y. T. Lee, and R. I. Kaiser, *J. Chem. Phys.* **110**, 7119 (1999).
- ⁴¹N. Balucani, O. Asvany, L. C. L. Huang, Y. T. Lee, R. I. Kaiser, Y. Osamura, and H. F. Bettinger, *Astrophys. J.* **545**, 892 (2000).